

# The high temperature interaction between molybdenum and graphite

R. B. MATTHEWS,\* G. M. JENKINS

*Department of Metallurgy and Materials Technology, University College of Swansea, UK*

This paper describes a series of experiments elucidating the interaction of molybdenum and graphite at temperatures between 2000 and 3000° C. The kinetics of the reaction were studied by a layer growth technique, perpendicular and parallel to the plane of deposition of a layered pyrocarbon. The variation of contact angle with temperature was measured optically. The behaviour of Mo wire embedded in natural graphite powder was studied. The electron microprobe was used to determine diffusion of Mo in C and C in Mo. Electron scanning was shown to be a powerful tool for following the movement of Mo particles on graphite surfaces. A model and related mechanism are proposed to explain these results. Additional work is reported to compare the above behaviour with the reaction of Mo with glassy carbon and other metals with pyrocarbon.

## 1. Introduction

Very little information is available about the nature of wetting of graphites by liquid metals. Munson [1] determined the surface energies of some liquid metal interfaces with carbon, and Buhsmer and Heintz [2] applied classical wetting theory to some non-reactive liquid metal-graphite systems.

Another aspect of carbon-metal interactions is the high-temperature diffusion between carbon and metallic materials. Carbon, being a relatively small atom, should travel rapidly through metal and carbide lattices via interstitial vacancies. On the other hand, the transport of metal atoms through graphitic materials is thought to be a comparatively slow and difficult process.

Wolfe *et al.* [3] used tracer techniques to determine diffusion coefficients and activation energies for Ag, Ni, U and Th, diffusing through pyrographite, dense polycrystalline graphite and porous polycrystalline graphite. The activation energy for diffusion in pyrographite parallel to the *c*-axis was somewhat greater than that parallel to the *a*-axis, while diffusion coefficients measured in the *a*-direction were an order of magnitude greater than in the *c*-direction. Diffusion parallel to the *a*-axis progressed via the boundaries between

growth cones. When pyrographite was annealed to eliminate the cone structure, the diffusion coefficients were reduced by several orders of magnitude. Diffusion coefficients were identical in the dense and porous graphites, but activation energies were generally greater for polycrystalline graphites than for pyrographite. Uranium migrated as a carbide, indicating that the metallic atoms are diffusing and precipitating as UC<sub>2</sub>. Consequently, there should be a small amount of atomically dispersed U in the graphite matrix. The authors conclude that metallic diffusion in all types of graphites proceeds via grain boundaries and substructure boundaries. They propose a diffusion model in which the diffusing atoms are bound in "traps" separated by regions over which the metal atom can move rapidly. The authors visualize these "traps" to be unsatisfied carbon atom bonds at defect boundaries which will readily form bonds with, and "trap", the diffusing metal atoms. Basal plane surfaces correspond to the regions offering little resistance to diffusion.

The diffusion of carbon in carbides can be estimated by a layer growth technique. When carbide-forming metals react with carbon at high temperatures, the growth of the various carbide layers can be measured by metallographic techniques. The

\* Present address: Atomic Energy of Canada Ltd, Pinawa, Manitoba, Canada.

carbide interfaces follow a parabolic growth rate, therefore, by applying classical kinetics and diffusion theory, a diffusion coefficient for carbon diffusion in each carbide layer can be determined. The validity of this method depends on several limiting assumptions: (1) the layer growth must occur by carbon diffusion alone; (2) there must be no appreciable metal diffusion into the carbon; and (3) the diffusivity must be independent of composition variations within each layer. Resnick *et al.* [4] used this technique to determine the diffusivity of carbon in tantalum and columbium carbides. Adelsberg *et al.* [5] found that the growth of ZrC was controlled by carbon atom diffusion through the carbides to the metal-carbide interface. Tobin *et al.* [6] proposed that the carbon diffused through ZrC by jumping between vacant octahedral sites by passing through a tetrahedral site. Brizis *et al.* [7] studied the layer growth of niobium carbides, and Adelsberg and Cadoff [8,9] examined the reaction kinetics between carbon and titanium, and vanadium. Basically these studies led to the same conclusions: (1) carbide layer growth increased linearly with the square root of time; (2) carbon diffusion through the carbides was the rate-controlling mechanism; and (3) carbon atoms diffused interstitially.

Sarian and Criscione [10] pointed out that several processes could contribute to the carbide layer growth and the technique could not distinguish between them. The authors used tracer methods to measure the diffusion of carbon in ZrC. They noted that grain-boundary diffusion contributed significantly and that back-diffusion of Zr could not simply be ignored. The authors suggest that simple mechanistic models derived from the layer growth technique may not be entirely valid.

## 2. Mo-C diffusion studies

Since no information was found on the molybdenum-carbon system, it was decided to investigate the kinetics of the Mo-C reaction at the temperatures of interest to a programme aimed at dispersion-hardening graphite [11, 12]. Initially, it was attempted to measure the reaction between Mo and compacted natural graphite surfaces; however, the zone interfaces were very indistinct and uneven. It was necessary to use pyrocarbon as the carbon source. It was assumed that the Mo-C reaction zones parallel and perpendicular to the deposition plane would represent the Mo-natural

graphite reaction zones.

Diffusion couples were prepared by placing slices of 5 mm diameter Mo rod (99.95% Mo) onto specimens of as-deposited pyrocarbon accurately machined so that the face in contact with the Mo slice was either parallel or perpendicular to the plane of deposition. The contacting surfaces were ground flat and polished to ensure contact. The couples were placed in the hot zone of a graphite resistance furnace and heat-treated in an inert atmosphere for various time periods up to 64 min at 1915, 2015, 2115 and 2170°C. The heating rates were kept constant at each temperature, and the samples were furnace cooled. After heat-treatment, the couples were sectioned, polished and etched to reveal the carbide zones. The zone depths were measured on a Vickers Metallograph using a measuring eye piece over several points at the interfaces.

Fig. 1 shows the zones at 2115°C and 36 min. Because carbon atoms are more easily detached from the edges rather than the centres of the

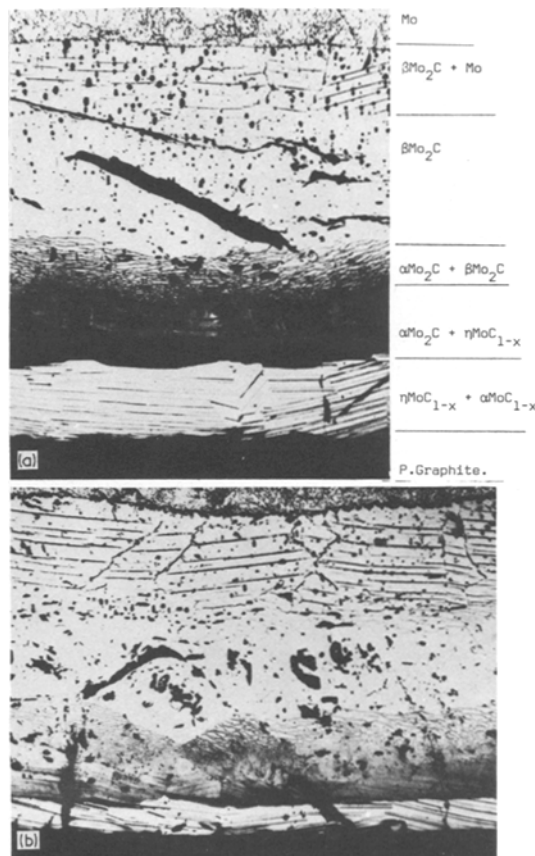


Figure 1 Molybdenum-pyrocarbon diffusion couples after 2115°C and 36 min,  $\times 120$ , Murakami's etch. (a) Perpendicular, (b) parallel, to the *c*-axis.

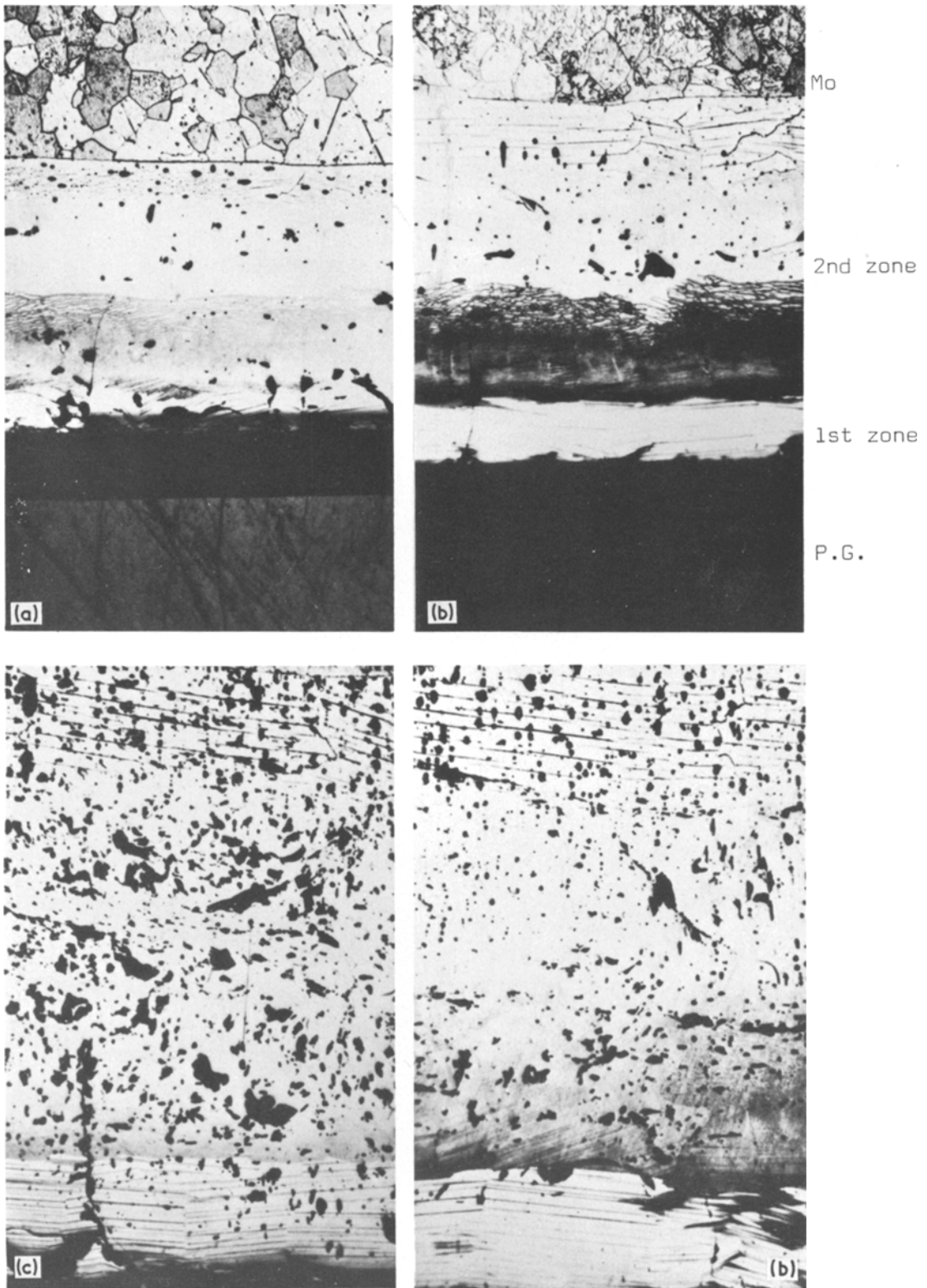


Figure 2 Molybdenum–pyrolytic carbon diffusion couples perpendicular to *c*-axis, 2115°C, ×100, Murakani's etch. (a) 9 min, (b) 16 min, (c) 49 min, (d) 64 min.

graphite sheets, the reaction zones are deeper perpendicular to the *c*-axis. The zones are identified according to Rudy *et al.* [13] in agreement with the Mo-C phase diagram. The overall reaction zone is rather complex with numerous phases present, however, the basic zone interfaces between MoC<sub>1-x</sub> and Mo<sub>2</sub>C and between Mo<sub>2</sub>C and Mo are distinct and even. The diffusion zone has numerous voids and cracks in it due to (1) precipitation of primary graphite, (2) lattice shrinkage and (3) differential thermal expansion.

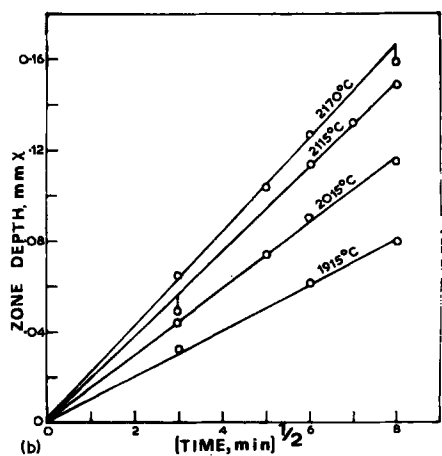
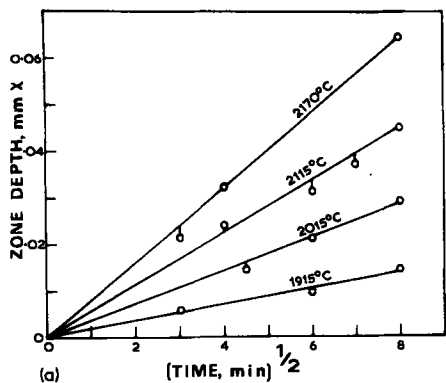
Fig. 2 shows the 2115°C series of diffusion zones normal to the *c*-axis. The measured MoC<sub>1-x</sub> zone is the bottom thin light band in each picture while the Mo<sub>2</sub>C zone extends to the last interface at the Mo-rich end. At each temperature a zero time run was made to correct for the heating and cooling times. According to Adelsberg *et al.* [5] the isothermal zone thickness can be determined by:

$$\chi^2 = x^2 - \frac{1}{2}x_0^2 = K_p t$$

where:  $\chi$  = isothermal zone thickness at time, *t*,  
*x* = measured zone thickness, *x*<sub>0</sub> = zone thickness at *t* = 0, *K<sub>p</sub>* = isothermal parabolic rate constant.

The data for the MoC<sub>1-x</sub> and Mo<sub>2</sub>C layer growth are plotted in Fig. 3a and b. A straight line relationship between  $\chi$  and *t*<sup>1/2</sup> results at all temperatures, and the rate constant, *K<sub>p</sub>*, can be determined from the slope of these lines at each temperature. When the rate constants are plotted as a function of temperature on Arrhenius plots (Fig. 4), straight lines result. The slope of the MoC<sub>1-x</sub> plot yields an activation energy of 500 kJ mol<sup>-1</sup>; the slope of the Mo<sub>2</sub>C plot yields an activation energy of 220 kJ mol<sup>-1</sup>. This difference seems to be extremely large (in contrast, Brizis *et al.* [7] found 325 kJ mol<sup>-1</sup> for Nb<sub>2</sub>C and 385 kJ mol<sup>-1</sup> for NbC).

The main interest is the overall reaction kinetics between graphite and the carbide particles at hot-working temperatures; consequently, the above results are probably not directly pertinent to real conditions. It was noticed on the sectioned diffusion couples that the Mo rod sank into the pyrocarbon a measurable distance. Since the Mo rods had a constant diameter, it was thought that the



(b)

Figure 3 Carbide layer thickness as a function of time and temperature. (a) MoC<sub>1-x</sub>, (b) Mo<sub>2</sub>C.

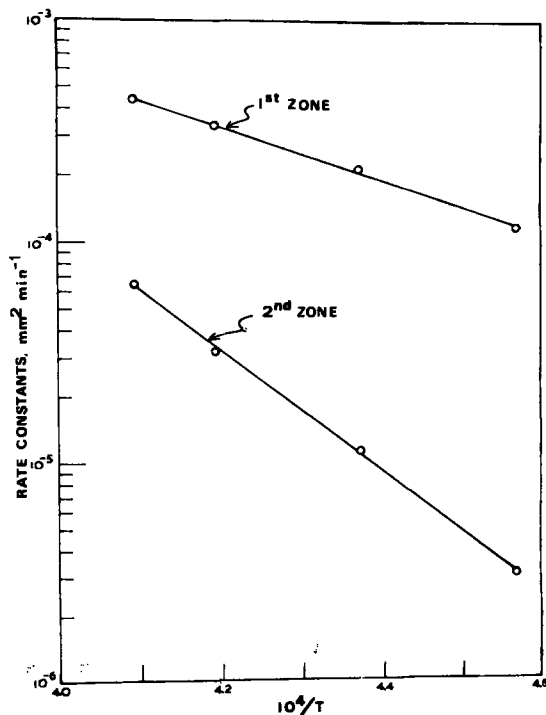


Figure 4 Rate constants for molybdenum carbide layer growth as a function of temperature.

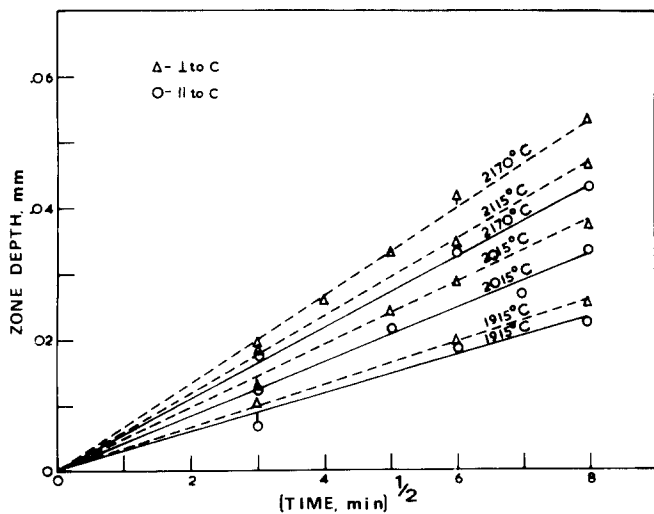


Figure 5 Penetration of molybdenum into pyrocarbon parallel and perpendicular to the graphite c-axis as a function of time and temperature.

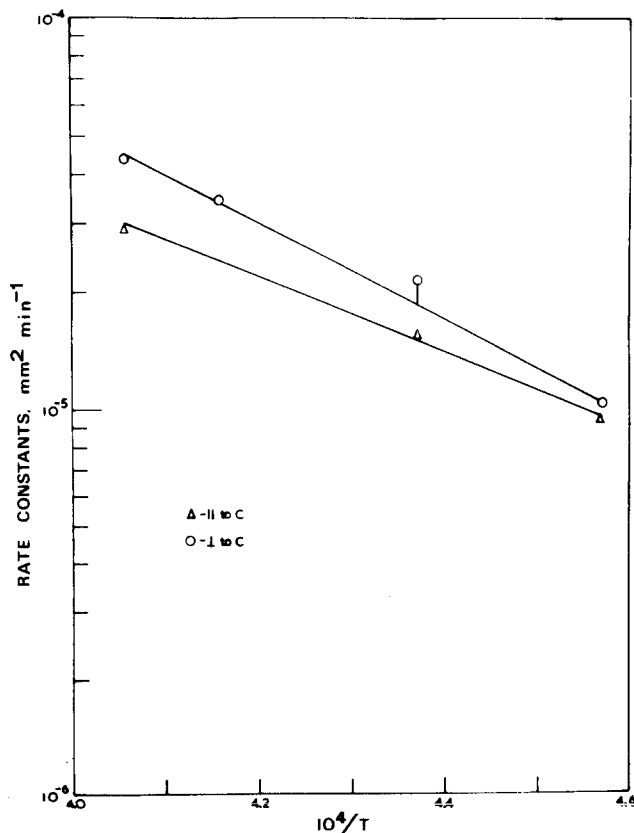


Figure 6 Rate constants of molybdenum penetration into pyrocarbon as a function of temperature.

change of depth of Mo penetration into the pyrocarbon as a function of time and temperature would give an indication of the total rate of the diffusion of carbon into molybdenum. A layer growth analysis was performed and the penetration

depths are plotted versus time in Fig. 5. Again parabolic growth rate is followed, and when the rate constants are plotted against reciprocal temperature in Fig. 6, a straight line activation curve results. The depth of penetration is greater perpen-

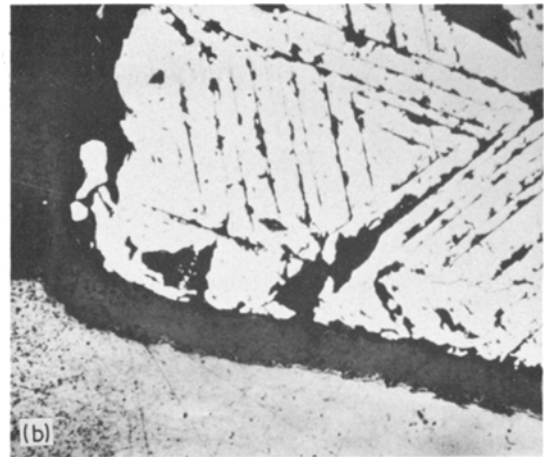
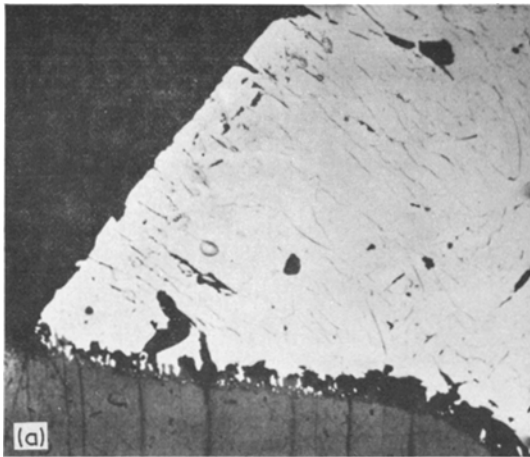


Figure 7 Molybdenum carbide-pyrocarbon wetting angle, H.T.T. 2525° C,  $\times 130$ . (a) Perpendicular to *c*-axis, wetting angle-55°; (b) Parallel to *c*-axis, wetting angle 81°.

dicular to the *C*-axis, and the activation energy for diffusion perpendicular to the *C*-axis is  $250 \pm 20$  kJ mol<sup>-1</sup> while parallel to the *c*-axis the activation energy is  $190 \pm 15$  kJ mol<sup>-1</sup>. Carbon atoms are more easily removed from the edge of basal planes than from the basal plane surface.

### 3. Mo-Graphite wetting studies

The layer growth technique was ineffective at temperatures greater than 2200° C because the Mo rod melted at the Mo-Mo<sub>2</sub>C eutectic temperature (2205° C) and the carbide layers were indistinguishable. Simple wetting studies were performed in order to classify the Mo-graphite interactions at the higher temperatures. When Mo-pyrocarbon dif-

fusion couples were heated to 2525° C for 30 min, typical sessile drops were formed as shown in Fig. 7. The contact angle between the carbide drop and the edges of basal planes is 54.8° while the contact angle on the basal surface is 81.0°. This difference is taken to be expected when one considers the large discrepancy between the two activation energies for Mo penetration parallel and perpendicular to the *c*-axis. Basically, carbon atoms at the basal plane edges react more readily than those in the basal surface. Perpendicular to the *c*-axis (Fig. 7a) a definite bond forms between the graphite and the carbide drop. There is an interaction zone separating the two phases, which contains small carbide particles in what appears to

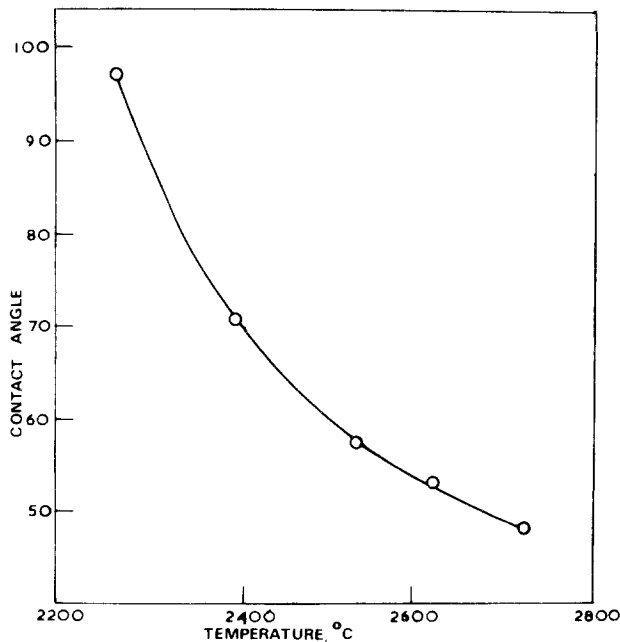


Figure 8 Variation of molybdenum carbide-natural graphite wetting angle with temperature.

be recrystallized graphite. Parallel to the *c*-axis (Fig. 7b) the drop is separated from the pyrocarbon basal surface, and no interaction zone can be seen.

The contact angles between natural graphite and Mo were measured at temperature by photographing the sessile drop through the furnace observation window. The sample was soaked at each temperature for 10 min, then photographed. The photographs were enlarged with a slide projector, and the contact angles measured on the projected image. The carbide angles are listed in

TABLE I Molybdenum carbide—natural graphite contact angles

Temperature (°C)	Contact angle
2280	96.6°
2390	70.4°
2525	56.4°
2625	52.8°
2730	48.2°
R.T.	43.2°

Table I and plotted versus temperature in Fig. 8. The contact angles drop rapidly between 2300 and 2500° C then decrease slowly up to 2730° C. The R.T. angle is the contact angle of the solidified drop measured after removing the sample from the furnace. The decrease in contact angle with temperature represents an increasing interaction between the two phases.

At 2525 and 2730° C a good bond formed with a deep reaction zone containing numerous isolated carbide particles. Recrystallized graphite particles were seen growing into the carbide, especially at 2730° C. It would seem that the liquid carbide is migrating through the graphite and renucleating into discrete particles. These micrographs also reveal that the graphite has fractured around the reaction zone. No doubt this fracture is due to the difference in thermal contraction between the carbide and the graphite, but it is significant that the reaction zone remains in contact with the carbide.

The data prove that the interaction of edge atoms proceeds more rapidly than the interaction of atoms from the basal surface. Quite simply the carbon atoms at the edges of basal planes will have unsatisfied primary bonds. Therefore, the dissolution of these atoms will be more energetically favourable than the dissolution of basal atoms with complete bonding. The wetting of pyrocarbon in Fig. 7 demonstrates the dissolution,

precipitation process more rapidly at the edges of basal planes. This difference can be attributed to the difference in surface energy resulting from the higher energy state of edge carbon atoms.

#### 4. Metal—graphite wetting and bonding investigations

A simple technique for observing the gross effects of heat-treatment and hot-working on the wetting and bonding phenomena has been developed. Sections of one millimeter diameter Mo wire (99.9% Mo) were cold-pressed with natural graphite powders into compacts. These compacts were heat-treated and hot-worked for 30 min at 1760, 2210 and 2525° C, then sectioned across the wire and polished. Photomicrographs of the polished sections are shown in Fig. 9. After heat-treatment at 1760° C (Fig. 9a) no bond is formed and the wire has separated from the graphite matrix. After heat-treatment at 2260 and 2525° C (Fig. 9b and c) the wire has formed an intimate bond with the graphite, and the interaction zone discussed in the previous section is again seen. Hot-work at 1760° C (Fig. 9d) seems to bring the two phases into contact but no interaction zone can be distinguished. Hot-work at 2270° C (Fig. 9e) deforms the wire and increases the depth of the interaction zone. Hot-work at 2525° C (Fig. 9f) further deforms the wire and also seems to increase the number of small carbide particles in the interaction zone. This sample was sectioned at a high angle so the wire is distorted, and the depth of the interaction zone is enhanced. Note the formation of voids in the centre of the heat-treated samples, this indicates some outward diffusion of Mo atoms. The network of cracks in the graphite matrix surrounding the wires further illustrates the strength of the bond between the carbide and the graphite.

Heat-treatment for 30 min at 2730° C (Fig. 10a) results in a reaction zone, parallel to the pressing direction, containing large particles. Hot-working under identical conditions increases the depth of the interaction zone and the number of small particles, (see Fig. 10b). Fig. 10c shows the interaction zone after hot-working, perpendicular to the pressing direction. The zone depth has increased over the parallel direction and there seems to be a greater density of carbide particles. Note that the carbide particle size decreases with distance away from the main interface. Precipitated primary graphite crystals can be seen at the interface and inside the carbide.

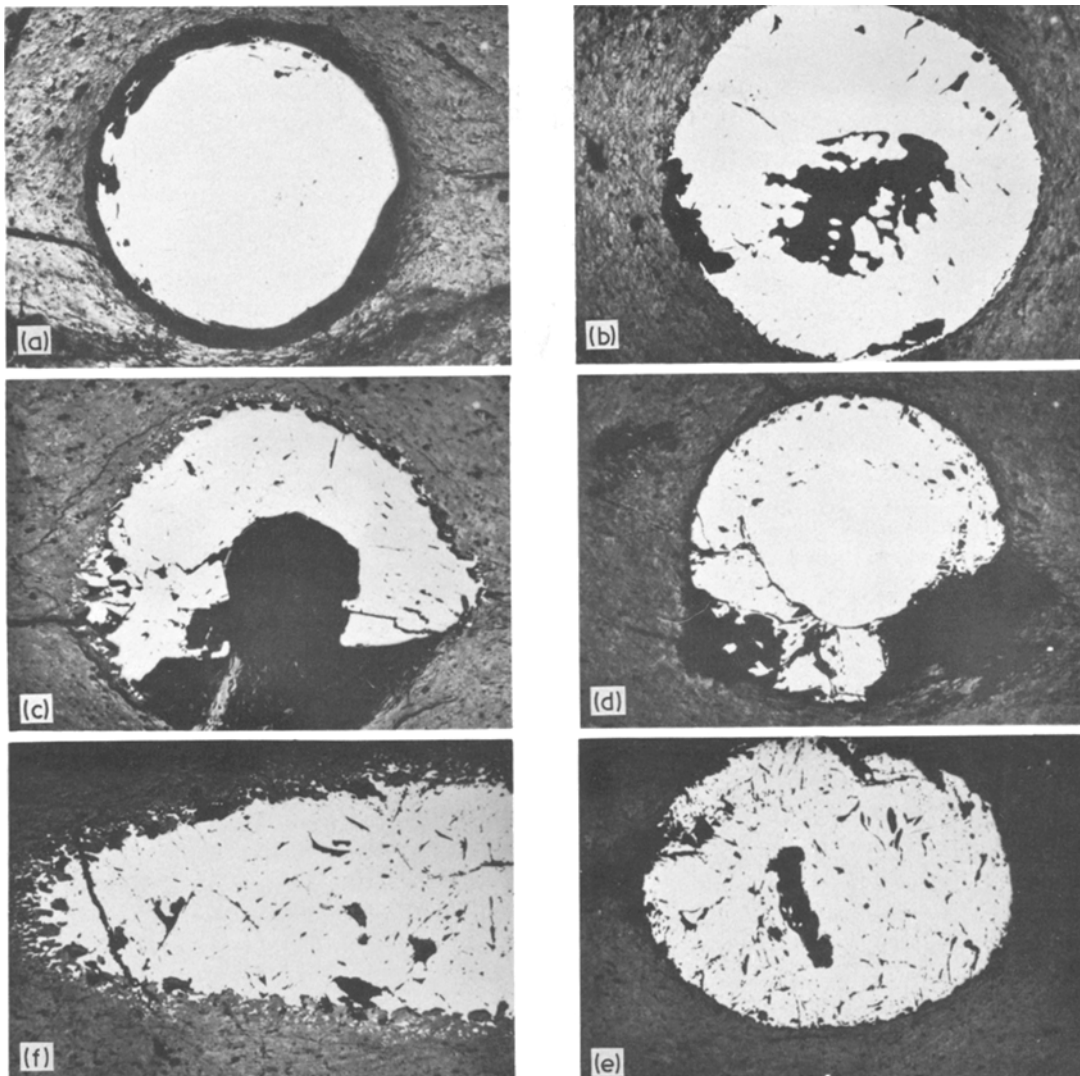


**Figure 9** Micrographs of Mo wire embedded in natural graphite after heat-treatment,  $\times 75$ . H.T.T: (a)  $1760^{\circ}\text{C}$ , (b)  $2270^{\circ}\text{C}$ , (c)  $2525^{\circ}\text{C}$ . H.W.T: (d)  $1760^{\circ}\text{C}$ , (e)  $2270^{\circ}\text{C}$ , (f)  $2525^{\circ}\text{C}$ .

A set of experiments identical to those previously discussed were performed with Ti (99.9%), and Nb (99.998%) wires at  $2525^{\circ}\text{C}$ . None of these samples showed any evidence of bond formation or even intimate contact between the carbides and graphite matrix. Centre voids were formed in many of the carbides and some distortion of the wire resulted from hot-working. In all cases, the wires shrank away from the graphite leaving a large gap between the two phases, although these metals do actually wet the graphite at temperature and then contract away upon cooling due to the lack of bond formation. This is not to say that hot-working these materials at temperatures greater than  $2525^{\circ}\text{C}$  would not strengthen them. White and Pontelandolfo [14] and Harada *et al.* [15]

prove that Zr and Nb are effective strengthening additions after hot-working at temperatures greater than  $3000^{\circ}\text{C}$ . Likewise, John [16, 18] has shown that Ti-natural graphite composites are significantly strengthened after hot-working at temperature in excess of  $2700^{\circ}\text{C}$ .

Previous investigators have assumed that the outward diffusion of metal atoms was negligible. They offered proof of this assumption by carburizing metal wires and noting that absence of central voids. Our wire experiments show that the opposite is true. When Mo, Ti, Zr and Nb wires were heat-treated in the presence of natural graphite, large voids were formed in the wire centres. This discrepancy lends support to the criticisms of the layer growth technique put forward by Sarian

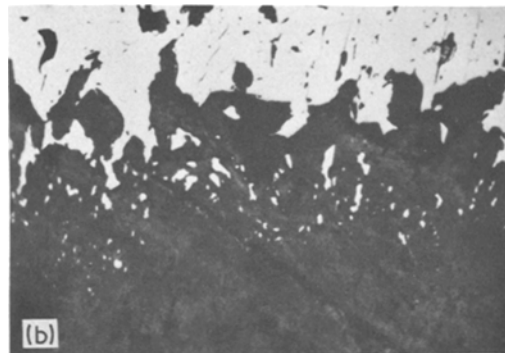
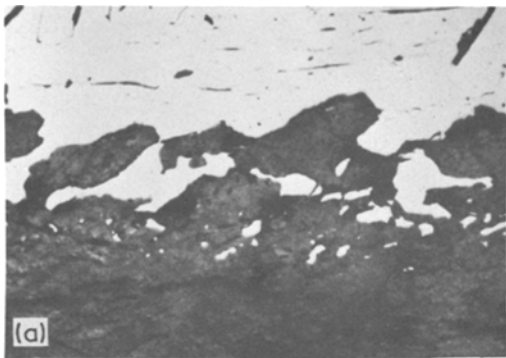
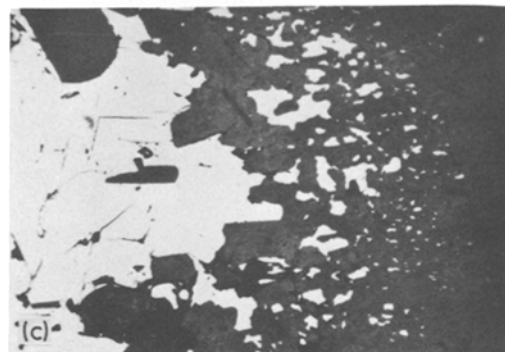


**Figure 10** Molybdenum carbide–natural graphite interface reaction,  $\times 300$ . (a) H.T.T.,  $2730^{\circ}\text{C}$ ,  $\parallel$  to pressing direction; (c) H.W.T.,  $2730^{\circ}\text{C}$ ,  $\perp$  to pressing direction.

and Criscione [10].

### 5. Bonding between natural graphite and molybdenum carbide particles

In order for a dispersed second phase to effectively strengthen a matrix material there should be an intimate bond formed at the interface between the two phases. This bond could be a simple mechanical bond, but preferably would involve mutual diffusion of the two species or some type of



chemical interaction. The presence of some sort of bond between massive molybdenum carbide and natural graphite has been established by optical observation in the previous section. However, this wetting-type bond does not necessarily exist on the submicroscopic scale at the carbide–graphite interface.

Harada *et al.* [15] used electron microprobe images of embedded carbide particles to illustrate the diffusion of the metal phase into the graphite matrix surrounding the particle, thereby establishing the possibility of a diffusion bond. Similar

**Figure 11** Electron microprobe images of carbide particles after hot-working at  $2270^{\circ}\text{C}$ ,  $\times 2000$ . (a) Electron image, (b) C, (c) Mo.

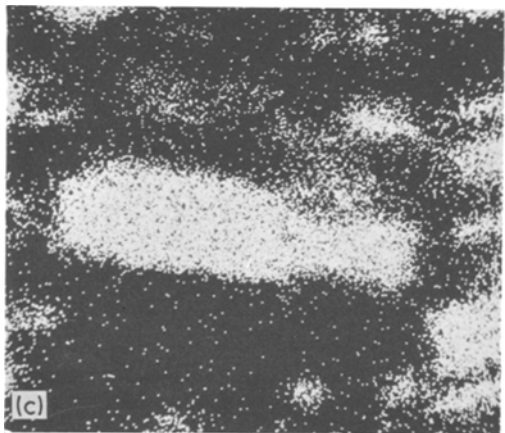
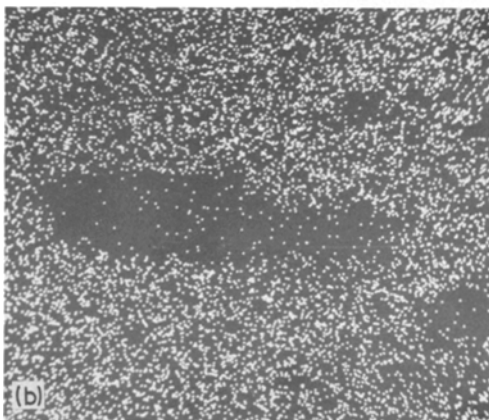
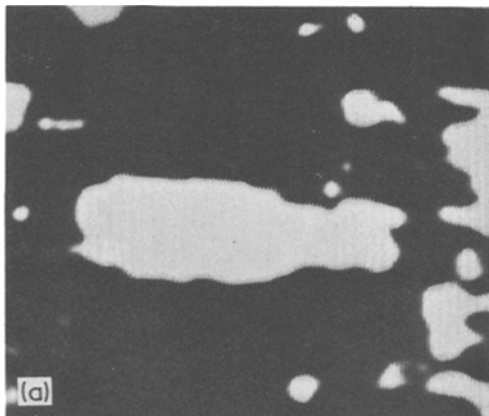




**Figure 12** Movement of molybdenum carbide particle on graphite basal plane after heat-treatment at 2525° C,  $\times 4000$ .

electron microprobe images of molybdenum carbide particles are shown in Fig. 11. The photomicrographs were taken of a polished section of a molybdenum–natural graphite composite hot-worked at 2270° C. Fig. 11a shows the electron image; Fig. 11b shows the carbon X-ray image;

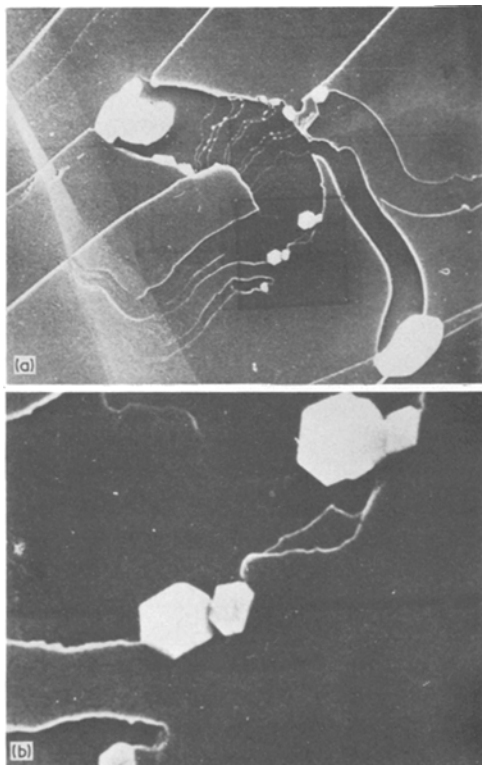


**Figure 13** (a) Carbide particles moving across basal plane edges. Note small carbide particles deposited at edges, H.T.T. 2525° C,  $\times 4000$ . (b) Hexagonal carbide particles attached to graphite basal plane edges from (a),  $\times 16\,000$ .

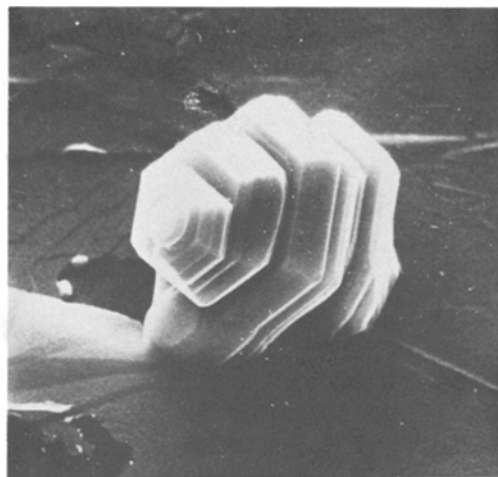


**Figure 14** Hexagonal molybdenum carbide particles protruding from basal plane surface,  $\times 10\,000$ .

Fig. 11c shows the molybdenum X-ray image. The white spots represent the concentrations of C and Mo. The most obvious conclusion from these probe pictures is that the Mo diffuses a finite distance away from the carbide particle into the graphite matrix.

## 6. Wetting and bonding

The interfacial reaction between two phases is probably the most critical when attempting to strengthen one phase with a dispersion of another. This means that there must be intimate contact between the surfaces of the two phases and preferably the presence of a chemical bond at the interface. The wetting and bonding experiments have proven that molybdenum carbide wets natural graphite at high temperatures and that there is an intimate interfacial bond between the two phases.

A final simple experiment has plainly demonstrated the nature of the carbide–graphite bond. Molybdenum powder, sprinkled on a graphite single crystal, was heat-treated at 2525° C. The surface was examined under the stereoscan. Fig. 12 shows a single particle on the graphite basal plane. Obviously the Mo particle has moved from A to B and transformed into a carbide during the heat-treatment. Carbon atoms have been dissolved into the molybdenum from the basal surface and whole sections of basal planes have been “eaten up” by the moving, transforming particle. The movement of the particle was probably facilitated by the presence of a layer of liquid from the Mo–Mo<sub>2</sub>C eutectic reaction. The particle in Fig. 13a has moved across several basal planes and deposited small carbide particles at the basal plane edges.

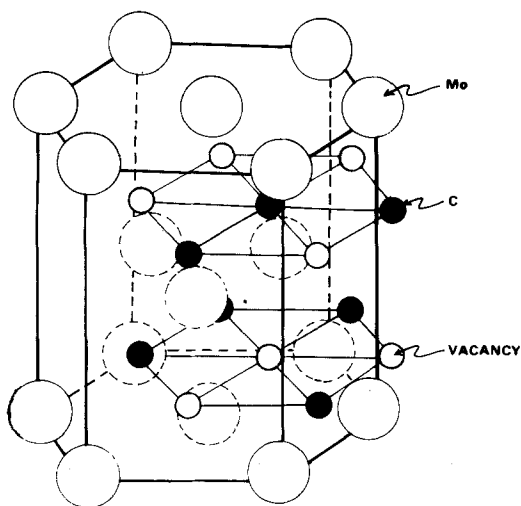


Figure 15 Schematic drawing of  $\text{Mo}_2\text{C}$  structure. Hexagonal close packed Mo atoms with carbon sublattice in octahedral voids.

Fig. 13b shows the carbide deposits at high magnification. Apparently they are hexagonal molybdenum carbides and they seem to be intimately attached to the edges of graphite basal planes. A singularly excellent hexagonal particle is observed protruding from the basal surface in Fig. 14.

This channelling is very similar to that observed at lower temperatures in an oxidizing atmosphere when Mo acts as a catalyst. However, the channels in our case are the same width as the crystal at the head of the channel, indicating no oxidation took place. Indeed, special care was taken to ensure that a high quality Argon atmosphere was maintained throughout, all residual oxygen being absorbed by the encompassing carbon black.

The  $\text{Mo}_2\text{C}$  structure is drawn in Fig. 15. The

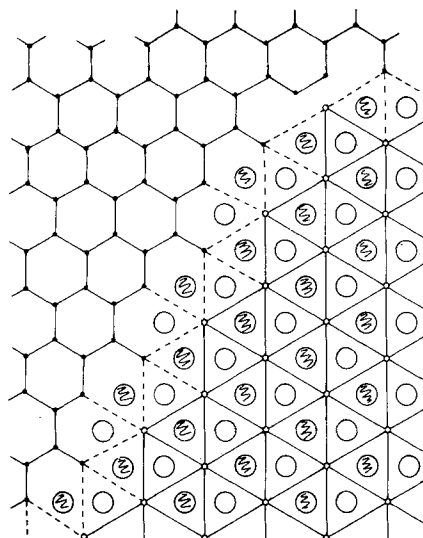
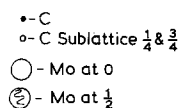


Figure 16 Schematic illustration of the atomic match between the graphite basal plane and the carbon sublattice in  $\text{Mo}_2\text{C}$ .

carbon sublattice consists of partially filled octahedral voids in the close-packed Mo lattice. Fig. 16 shows the atom positions in  $\text{Mo}_2\text{C}$  (looking down on the basal plane) in conjunction with the graphite basal structure. This diagram suggests that carbon atoms at basal plane edges match with nearly equivalent positions in the carbon sublattice of the  $\text{Mo}_2\text{C}$  structure. The distance between the octahedral voids is  $3.006 \text{ \AA}$  and the distance between opposing carbon atoms in the graphite hexagon is  $2.84 \text{ \AA}$ . With some surface distortion in the carbide lattice, an epitaxial fit can be visualized for short distances at the graphite- $\text{Mo}_2\text{C}$  interface. This atomic match clearly rationalizes the micrograph in Fig. 13b. Atomic fit along the  $c$ -axis is not so easily pictured, but Fig. 17 indicates a possible

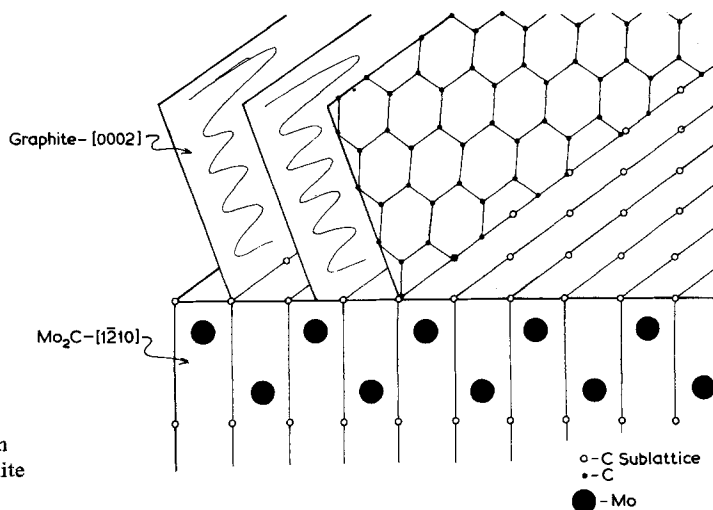


Figure 17 Further schematic illustration of the atomic match between the graphite lattice and the  $\text{Mo}_2\text{C}$  lattice.

arrangement. If the graphite lattice bonds to the  $\text{Mo}_2\text{C}$  crystal with the graphite sheets tilted at about  $19^\circ$  to the  $\bar{2}10$  planes of the  $\text{Mo}_2\text{C}$  lattice there is atomic match for every other graphite basal plane with the carbon sublattice. Such a small tilt angle may easily disappear with suitable local adjustment in the spacing between graphite sheets, which is easily accomplished in view of the weakness of bonding between such sheets.

The above discussion and diagram serve to demonstrate the possibility of the existence of a coherent bond between  $\text{Mo}_2\text{C}$  and graphite. The bond between the carbide dispersion and natural graphite is certainly a result of this atomic fit. It is impossible to say whether this bond involves electron transfer and chemical bonding. However, the low temperature stability of the bond and the cracking in the graphite matrix away from the interface indicates that the bond has some strength.

## 7. Interactions of molybdenum

### 7.1. Glassy carbon interaction

The glassy carbon–molybdenum interaction was cursorily investigated in parallel to Fitzer's work with vanadium [17]. A polished Mo rod was placed on a polished G.C.-30 disc and heat-treated at  $2730^\circ\text{C}$  for 10 min. The sessile drop shown in Fig. 18a resulted. The wetting angle is lower than those for comparable natural graphite or pyrolytic

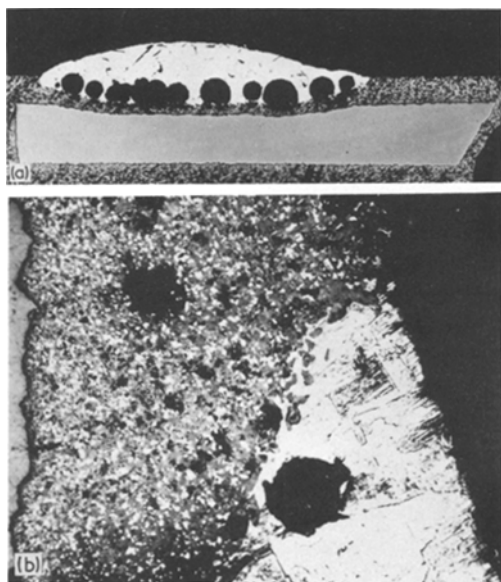


**Figure 18** Molybdenum–glassy carbon interaction after heat-treatment at  $2730^\circ\text{C}$ . (a)  $\times 10$ , to show that the whole specimen becomes coated with  $\text{Mo}_2\text{C}$ , and (b)  $\times 105$ , to show that the coating consists of a conglomerate of carbide particles and recrystallized graphite.

graphite samples and the interaction zone is amazingly large. A fine dispersion of molybdenum carbide has completely surrounded the surface of the G.C. disc via the dissolution precipitation mechanism. A high magnification micrograph in Fig. 18b shows the fine carbide dispersion in recrystallized glassy carbon and a decreasing particle size with depth of penetration.

It is interesting to relate this reaction with glassy carbon to the molecular structure of the carbon. Elsewhere [19], it has been shown that glassy carbon consists of ribbons rather than sheets of carbon atoms. Within ribbons strong C–C bonds exist akin to those in perfect graphite sheets. Only weak van der Waals bonding exists between ribbons which have a probability of stacking above each other to form microfibrils. Edge-to-edge bonding between ribbons in neighbouring microfibrils stiffens the material at room temperature and prevents ingress of foreign matter – thus preserving the characteristic chemical inertness of glassy carbon. Elsewhere [20], it has been shown that sodium and potassium vapour break through these barriers and causes a violent disruption as the foreign atoms intercalate between the graphite ribbons. To most other metals glassy carbon is inert. Above,  $2000^\circ\text{C}$  edge-to-edge bonding is overcome by thermal activation, allowing the material to creep under the influence of an applied stress. It is precisely at these high temperatures that molybdenum atoms begin to wet the glassy carbon and more rapidly to coat the whole specimen. We would surmise that at these high temperatures molybdenum atoms are able to travel along ribbon edges down into the body of the glassy carbon and simultaneously range rapidly over the whole of the exposed carbon surface.

### 7.2. Interaction with other metals

A set of experiments similar to the Mo powder–graphite basal surface interaction discussed in Section 6 was carried out using Ti, V, Nb, Ta, W, Fe and Ni powders. The powders were lightly sprinkled on graphite single crystals enclosed in a crucible, rapidly heated to  $2700^\circ\text{C}$  and furnace cooled. The surfaces were then examined in the scanning electron microscope. Fig. 19 shows the interaction between the various powders and the graphite surface. Apparently titanium carbide melts and readily spreads over the graphite (Fig. 19a) but the individual particles do not move over the surface. The cubic particles in Fig. 19b are prob-

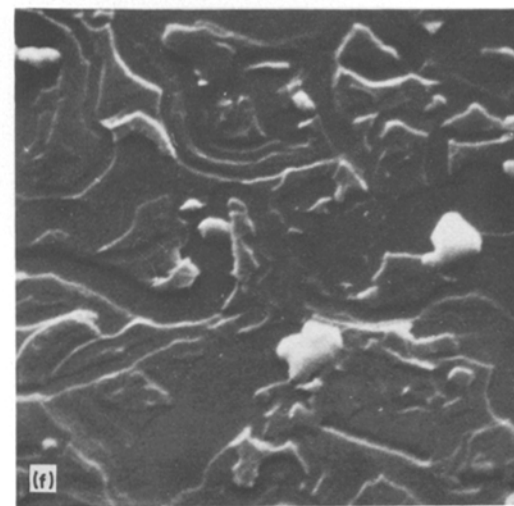
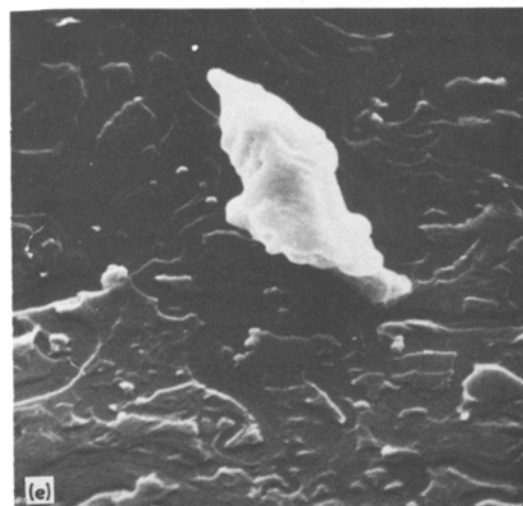
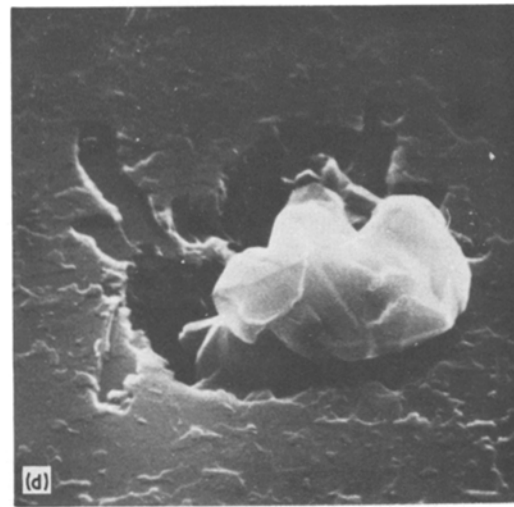
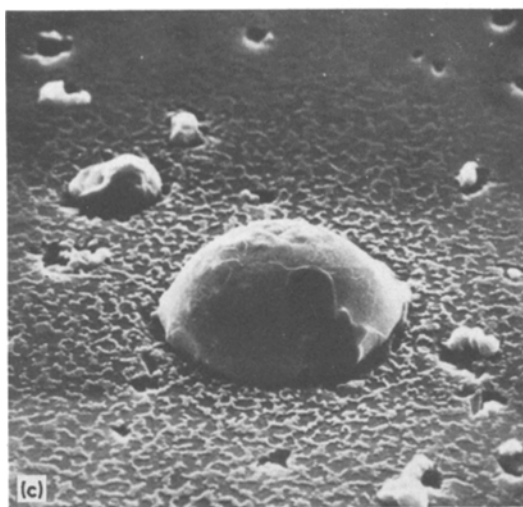
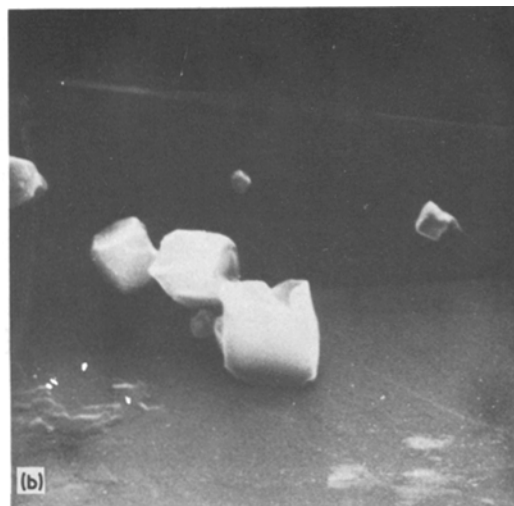
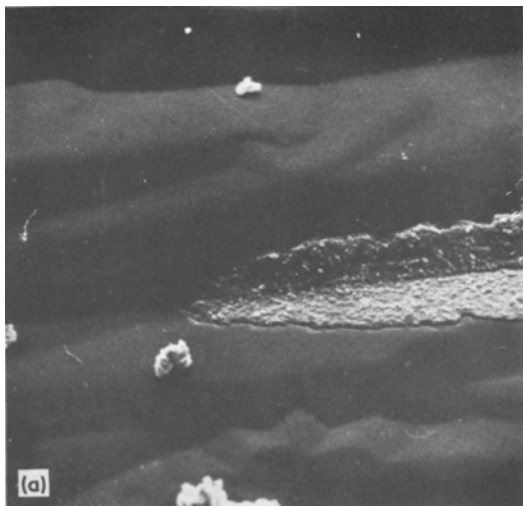


**Figure 19** Stereoscan micrographs illustrating interaction between various metal powders and graphite basal surface after heat-treatment at 2700° C. (a) Ti, ×1000; (b) Ti, ×4000; (c) V, ×1000; (d) V, ×5000; (e) Ni, ×4000; (f) Ni, ×8000, (g) Ta, ×2000; (h) Ta, ×8000; (i) W, ×8000, (j) Fe, ×2000; (l) Ni, ×1000.

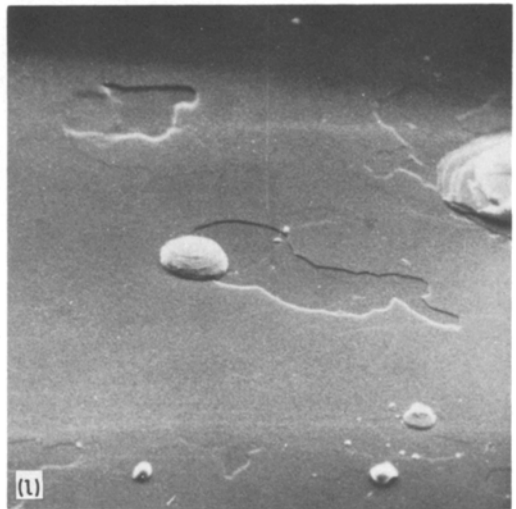
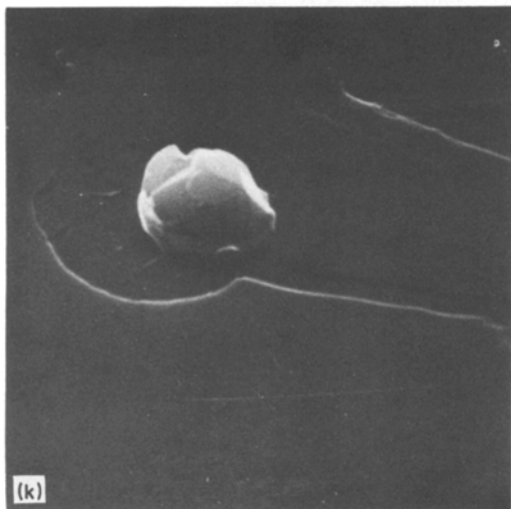
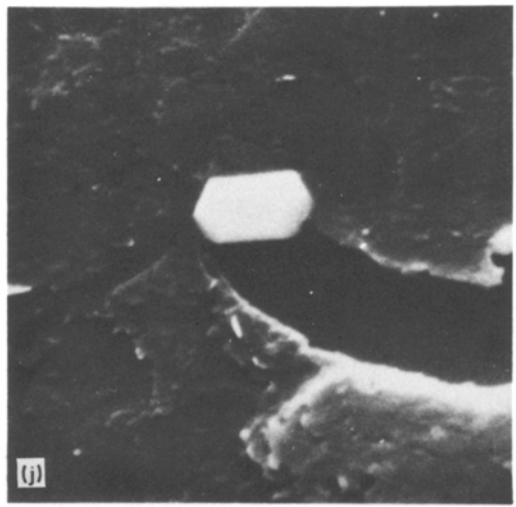
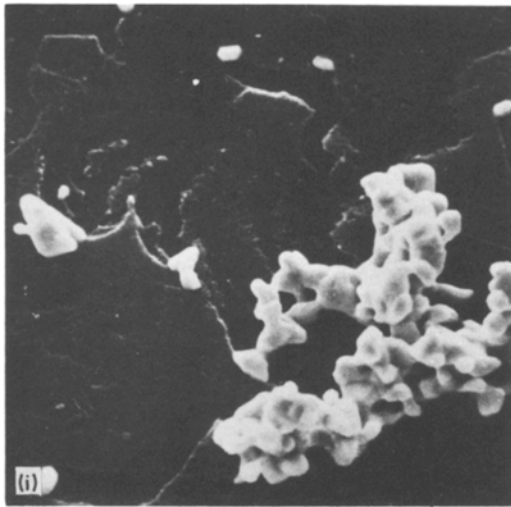
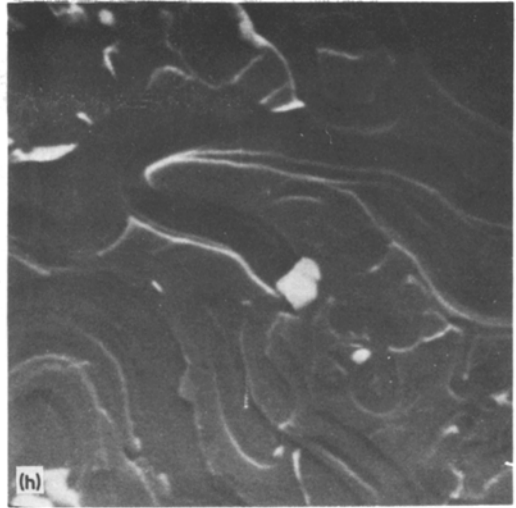
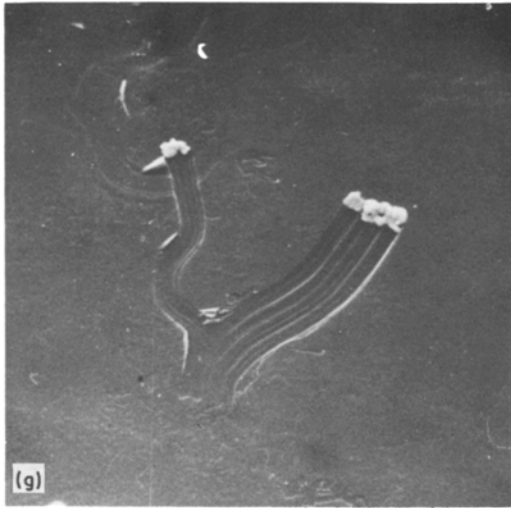


Figure 19 continued

ably TiC and no interaction with the graphite can be seen. Vanadium particles form droplets on the surface and seem to penetrate through the graphite (Fig. 19c and d). The graphite around the particles seems to have recrystallized.

Niobium, Ta (Fig. 19e to h) particles rapidly move over the basal plane surface and carve channels into the graphite, in a manner similar to Mo. Small particles seem to bond to the graphite but no epitaxial morphology is noticeable. Tungsten (Fig. 19i to j) behaves very similarly to Mo. The particles move over the surface and form hexagonal carbides whose *c*-axis are coincident with *c*-axis of the graphite. These micrographs imply that tungsten would be a good strengthening addition to natural graphite. Iron and nickel interactions are shown in Fig. 19k and l. Again the particles migrate over the graphite and carve channels into the surface.

Obviously more extensive work would be necessary to accurately interpret these micrographs, but the simple technique would seem to be an interesting method for studying metal-graphite interaction.

## 8. General conclusions

The interfacial interaction between graphite and molybdenum, as measured by diffusion, wetting and bonding experiments, has been shown to vary with the orientation of the graphite. Interaction is more rapid parallel to the graphite sheets because of the free bonding available at peripheral carbon atoms and the ease with which they can be detached. The strength of attachment between graphite edges and the carbide product is attributed to a merging of the graphite sheets in the graphite with the carbon sub-lattice in the Mo<sub>2</sub>C lattice. Only tungsten of the other metals examined seems to produce a carbide showing such epitaxy.

It has been demonstrated elsewhere [11] that molybdenum carbide, in the form of a fine dispersion promoted by hot-working, is effective in bonding together graphite flakes in a composite, thus inhibiting basal slip and fracture at room temperature. This results in an enormous increase in strength in what is still, essentially, a graphite matrix. The plasticity of Mo<sub>2</sub>C above 1800°C allows specimens to be moulded between graphite dies.

The wetting, bonding and dissolution/precipitation mechanisms that have been demonstrated for the molybdenum-graphite system suggest possible joining techniques for all graphite bodies.

## Acknowledgement

The authors wish to acknowledge the support of the Procurement Executive of the Ministry of Defence.

## References

1. R. A. MUNSON, *Carbon* **5** (1967) 471.
2. C. P. BUHSMER and E. A. HEINTZ, *J. Metals. Sci.* **4** (1969) 592.
3. J. R. WOLFE, D. R. MCKENZIE and R. J. BORG, *J. Appl. Phys.* **36** (1965) 1906.
4. R. RESNICK, R. STEINITZ and L. SEIGLE, *Trans. Met. Soc. AIME.* **233** (1965) 1915.
5. L. M. ADELSBERG, L. H. CADOFF and J. N. TOBIN, *ibid* **236** (1966) 972.
6. J. M. TOBIN, L. M. ADELSBERG, L. H. CADOFF and W. F. BRIZES, "Proceedings of the Conference on Nuclear Applications of Nonfissionable Ceramics" (American Nuclear Society, 1966) p. 257.
7. W. F. BRIZIS, L. H. CADOFF and J. M. TOBIN, *J. Nuclear Mats.* **20** (1966) 57.
8. L. M. ADELSBERG and L. H. CADOFF, *Trans. Met. Soc. AIME.* **239** (1967) 933.
9. *Idem*, *J. Amer. Ceram. Soc.* **51** (1963) 213.
10. S. SARIAN and J. M. CRISCIONE, *J. Appl. Phys.* **38** (1967) 1794.
11. R. B. MATTHEWS, D. B. FISCHBACH and G. M. JENKINS, Proceedings of the Third S.C.I. Carbon Conference, London (1970) p. 515-19.
12. R. B. MATTHEWS, Ph.D. Thesis, University of Wales (1970).
13. E. RUDY, S. T. WINDISCH, A. J. STONSICK and J. P. HOFFMAN, *Trans. Met. Soc. AIME.* **239** (1967) 1247.
14. J. L. WHITE and J. M. PONTELANDOLFO, *Carbon* **4** (1966) 305; *Nature* **269** (1966) 1018; *Carbon* **6** (1968) 1.
15. Y. HARADA, S. A. BORTZ and S. L. BLUM, "Fabrication and Characterization of Metal Carbide-Graphite Composites", Paper 38, Plansee Conference (1968).
16. D. JOHN, M.Sc. Thesis, University of Wales (1972).
17. E. FITZER and B. KEGEL, *Carbon* **6** (1968) 433.
18. G. M. JENKINS and D. JOHN, Proceedings of the Fourth S.C.I. Conference on "Industrial Carbon and Graphite", London (1974), Paper 123 pp. 207-8, "Extended Abstracts".
19. G. M. JENKINS, K. KAWAMURA and L. L. BAN, *Proc. Roy. Soc. A* **237** (1972) 501.
20. M. K. HALPIN and G. M. JENKINS, *ibid* **313** (1969) 421.

Received 1 August 1974 and accepted 23 May 1975.